

Areal Density Measurement of Imploded Cryogenic Target by Energy Peak Shift of DD-Produced Protons

Y. Kitagawa, K. A. Tanaka, M. Nakai, T. Yamanaka, K. Nishihara, H. Azechi, N. Miyanaga, T. Norimatsu, T. Kanabe, C. Chen, A. Richard,* M. Sato, H. Furukawa, and S. Nakai

Institute of Laser Engineering, Osaka University, Yamada-oka, Suita, 565, Japan

(Received 22 May 1995)

DD-produced protons are used to measure the imploded fuel-shell areal density $\rho\Delta R$. Twelve green beams of the GEKKO XII laser directly imploded a cryogenic foam-shell target containing a liquid or solid D_2 fuel. The proton emission is detected through a dipole magnet on a CR-39 plate, whose energy shift from 3.02 MeV yielded the maximum $\rho\Delta R$ of 10 mg/cm² or the density of 6 g/cm³, in agreement with that from the secondary neutron method within a factor of 2. The proton energy spread is sensitive to the laser energy imbalance.

PACS numbers: 52.70.Nc, 52.25.Tx, 52.50.Jm, 52.58.Ns

If fuel is compressed to about 1000 times the DT liquid density and a central region is heated more than 5 keV during the final implosion stage, a fuel ignition and a net energy gain will occur. Directly driven targets have reached imploded density of 200 times the liquid DT with glass microballoons [1] and 600 times with plastic hollow shell targets [2]. A high gain target will be a cryogenic DT hollow shell with a central cavity [3]. Since a central cavity of the cryogenic target has no residual gases, it achieves high density compression. We are studying density and areal density of imploded cryogenic D_2 targets. Very light plastic foam shell is used to help liquid or solid fuel make a uniform hollow shell. The secondary neutron method is used to determine the compressed density [4]. Neutrons from our cryogenic target, however, are few so we developed the other method to cross-check the areal density of the compressed shell. Fusion produced protons are used to measure the areal density.

The target that we used is a low density plastic foam hollow shell sphere. The foam layer contains a liquid or solid D_2 fuel, making a hollow shell cryogenic fuel target [5,6]. The foam is made of trimethylolpropane-trimethacrylate (typically $H_{14}C_{10}O_4$) of $10 \pm 1.3 \mu\text{m}$ thickness and $220 \pm 28 \text{ mg/cm}^3$ density (20% weight of solid plastics) and is coated with a $4 \mu\text{m}$ thick polyvinylphenol ablator, both to increase laser absorption and to reduce preheating [7]. The shell radius is within $R_0 = 303 \pm 24 \mu\text{m}$. The mass is $7.9 \pm 1.4 \mu\text{g}$. D_2 density at 21 K is 170 mg/cm^3 . The target is sustained vertically with $7 \mu\text{m}$ thick glass fiber at the center of the vacuum chamber and is cooled down to a presumed temperature in a retractable liquid-He-cooled shroud [8]. Once D_2 gas becomes liquid or solid in the foam layer, the shroud is retracted, and in 10 ms, 12 laser beams illuminate the target. At each exit of beams from the GEKKO XII system, there are a random phase plate and a single potassium dihydrogen phosphate crystal for second harmonics. The beams of 32 cm in diameter

are focused in tetrahedral configuration on the target by $f/3.15$ aspheric lenses. The focusing depth $d/R_0 = -5$. The total energy (527 nm) on target is from 3.5 to 12.1 kJ in $2.05 \pm 0.25 \text{ ns}$ quasi-flat-top pulse with $0.94 \pm 0.014 \text{ ns}$ rise. Energy imbalance σ_{rms} between 12 beams is $(3.7 \pm 1.7)\%$ rms for all of the shots.

In the final stage of implosion, a colder but denser main fuel-plastic mixed plasma layer (the second layer) will surround a central hot core (the first layer). In the hot core, deuterons collide and fuse each other, yielding two groups of fusion products: $T(1.01 \text{ MeV}) + p(3.02 \text{ MeV})$ and ${}^3\text{He}(0.82 \text{ MeV}) + n(2.45 \text{ MeV})$. In the second layer, tritons collide with deuterons, producing secondary neutrons (14.1 MeV). A yield ratio of secondary neutron to primary neutron gives the second layer (main fuel) $\rho\Delta R$, where ΔR is the thickness of the second layer [9]. The protons as well run through the second layer plasma, losing their energies. The resulting proton energy spectrum provides $\rho\Delta R$. For the first time, we successfully used the proton spectrum to estimate the imploded fuel-shell $\rho\Delta R$. The obtained $\rho\Delta R$ agrees within a factor of 2 with that from the secondary neutron method.

By the secondary neutron, we have measured $\rho\Delta R$ of compressed fuels in the intermediate density ($1\text{--}50 \text{ g/cm}^3$) region [4]. As a practical problem, cryogenic equipment inside the implosion chamber scatters both primary and secondary neutrons, decreasing detectable yields and increasing spurious γ -ray noises. These points may have the secondary neutron method fall short of the detection purpose. Here we try to cross-check the areal density by the new proton method. Fewes *et al.* have first detected energy spectra and stopping powers of protons on CR-39 plastics to probe laser plasmas from the NUHART target [10]. The proton spectrum method does not require any absolute number of emitted protons but their energy shifts. CR-39 plastics is not affected by γ -ray noises. These are the two advantages over other methods of measuring fuel areal density, such as secondary neutron or knock-on methods [11].

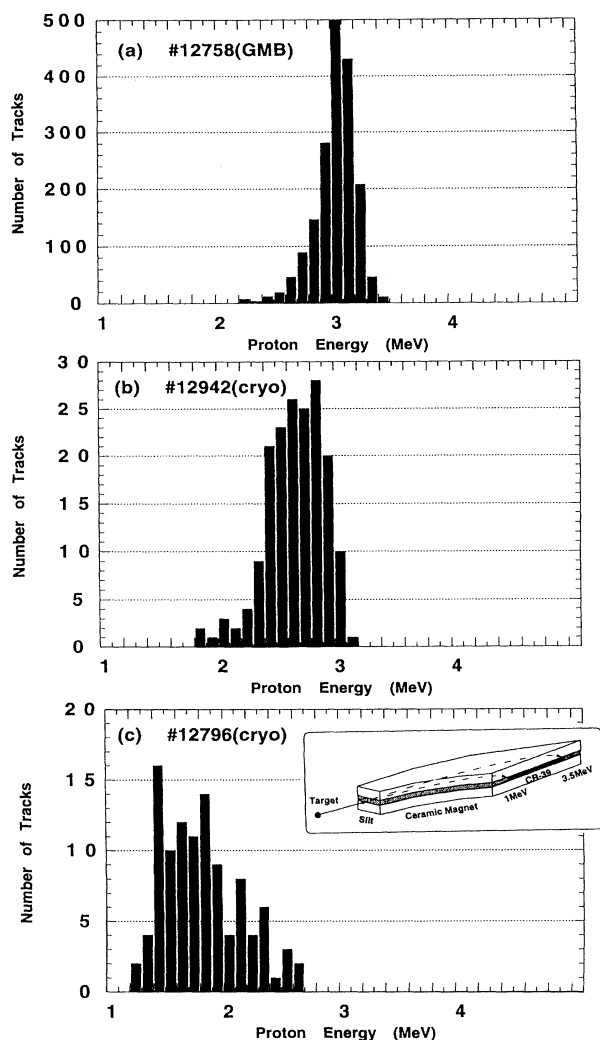


FIG. 1. Proton spectrum from (a) D₂-filled glass microballoon (GMB: 12758); (b) cryogenic foam-shell targets containing gas-liquid D₂ 12942, and (c) 12796. The diagram is the proton spectrometer.

A couple of scintillator-photomultiplier pairs [4] measured the primary neutrons at 1.71 and 1.15 m from the target. Another scintillator at 16.14 m from the target measured the neutron time of flight (TOF) temperature *T* to be between 0.12 and 2.5 keV. Neutron yield (NY) seems to

be in proportion to *T*^{0.5}. A 1D hydrocode HISHO simulated the maximum deuteron temperature to be about 1.9 keV in the first layer. NY is close to the simulation at the timing when the ingoing shock wave secondly meets the center. The NY error is about 10% between the two detectors. The other group of four scintillator-photomultiplier pairs is distributed at equal distances (28 cm) from the target and measures the secondary neutrons.

A newly developed proton spectrometer uses a ceramic dipole magnet (TDK: REC-22) of 7 kG. An entrance slit into the spectrometer is 0.5 mm wide and 2 mm long, and is set 15.3 cm away from the target. A CR-39 plate of 2 mm width and 40 mm length detects protons of 1–3.5 MeV. The countable limit is 1 count/channel of 100 keV width. Including particle divergences inside the spectrometer, the effective detection angle is 3.4×10^{-6} sr. The diagram is seen in Fig. 1. Figure 1(a) shows a proton spectrum from a D₂-filled glass microballoon (GMD: 12758) for comparison. As listed in Table I, the energy peak shift from 3.0 MeV is 0.085 MeV, and the energy spread is 0.3 MeV (Gaussian width). A source temperature of 1 keV can yield Doppler broadening of about 0.1 MeV [12]. The GMB energy spread, after subtracting the Doppler broadening, gives us an energy resolution of the spectrometer of $0.28 \text{ MeV}/3 \text{ MeV} = 9\%$. The spectra in Figs. 1(b) and 1(c) are from the cryogenic targets, as in Table I. By Gaussian fitting the spectra, we estimated both the peak shifts and the spreads. The number of tracks should be 3.4×10^{-6} times NY, assuming isotropic emission all over the angle. The protons may be affected not only from the inner plasma fields but also from the outer field, such as a self-generated magnetic field. The field attains a few hundred Gauss [13]. If the outer fields scatter or distort proton orbits, the number into the spectrometer might be affected and might not be proportional to NY. Nevertheless, as seen from Table I, the GMB and cryogenic target tracks are almost all within 50% of the expected yield, which suggests that the tracks reflect the history inside the targets to some extent.

The stopping power of a 3 MeV proton in a hot dense plasma is given by [14]

$$\frac{dE}{ds} = \frac{Z_0^2 e^2}{2\pi^2 v} \int dk \frac{\mathbf{k} \cdot \mathbf{v}}{k^2} \text{Im} \frac{1}{\epsilon(k, \mathbf{k} \cdot \mathbf{v})}, \quad (1)$$

TABLE I. Some shot data for D₂-filled GMB (12758) and foam cryogenic (12796–12942) targets. Initial fuel temperatures are 20–22 K.

Shot No.	Laser	Diam (μm)	D ₂ (atm)	DD neutron	Neutron ρΔR	Proton tracks	Proton shift	Proton ρΔR (mg/cm ²)	Compressed ρ (g/cm ³)
12758	7.3	621	11	7.0×10^8	2.7 ± 0.3	1807	-0.085	1.5 ± 0.5	0.05 ± 0.02
12796	7.8	590	100	5.66×10^7	6.3 ± 2.6	135	-1.21	10.5 ± 3.3	5.2 ± 0.6
12865	8.3	702	80	4.90×10^7	5.1 ± 4.6	99	-1.00	9.0 ± 3.9	3.9 ± 0.7
12874	12.1	612	84	5.57×10^8	5.4 ± 2.3	213	-1.16	10.3 ± 3.4	6.1 ± 0.9
12942	9.0	580	100	9.62×10^7	5.8 ± 2.6	175	-0.45	4.3 ± 2.4	1.6 ± 0.3

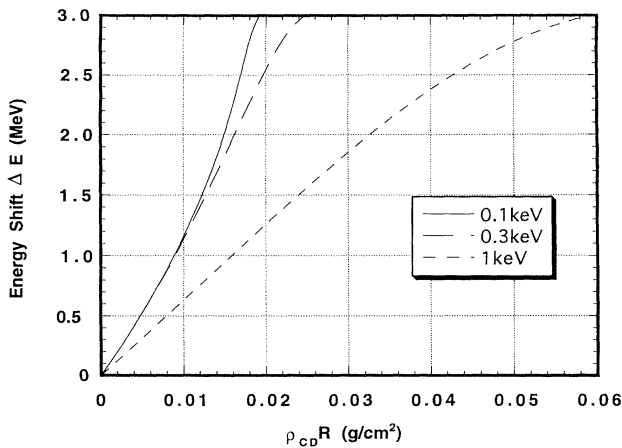


FIG. 2. Proton energy shift ΔE from 3.02 MeV, calculated versus 80% D_2 -200% CHO mixed plasma areal density ρR . $T_e = T_i = 0.1, 0.3,$ and 1 keV for the plasma density = 10 g/cm^3 .

where s is a distance and Z_0 is the atomic number of a test particle (proton) moving with a velocity v . The dielectric function $\epsilon(k, \mathbf{k} \cdot \mathbf{v})$ is simplified for our parameters as [14] $\epsilon^{-1}(k, \mathbf{k} \cdot \mathbf{v}) = 1 + 4\pi e^2 \chi_e^{(0)}(k^2 - 4\pi e^2 \chi_e^{(0)})^{-1}$, where $\chi_e^{(0)}$ is a zeroth order free electron susceptibility. Free electrons dominate in this case. Integrating Eq. (1) as for E from initial energy to zero, we obtain proton peak energy shift ΔE as a function of ρR . The result is plotted in Fig. 2 for 80% D_2 -20% CHO mixed plasma of the temperatures $T_e = T_i = 0.1, 0.3,$ and 1 keV at a density of 10 g/cm^3 . For the same ΔE , ρR is about 80% of that of pure D_2 plasma. The curves are not sensitive to the temperature below 0.5 keV. In Fig. 2, maximum ΔE of 3 MeV yields the upper limit of detectable $\rho R \approx 50$ mg/cm^2 , close to the limit of the secondary neutron method.

Fitting the peak shift of each shot to the curve for $T_e = 0.3$ keV in Fig. 2, we obtained $\rho \Delta R$ and plotted it as a function of the initial fuel temperature in Fig. 3. We also plotted $\rho \Delta R$ from the secondary neutron method by using the calculated temperature of 0.3 keV in the cold fuel layer (the second layer). The error bar on the proton is from the spectral spread, and the error bar on the neutron is from data scattering between four scintillators. We obtained the maximum fuel $\rho \Delta R = 10.5 \pm 3.3$ mg/cm^2 for shot No. 12796. To this shot, the secondary neutron provides 6.3 ± 2.6 mg/cm^2 . The proton and neutron data agree within a factor of 2 of each other, except that the error bars are so large. The lower the cryogenic temperature, the higher the compressed fuel $\rho \Delta R$ should be. Regrettably, cold fuels below the solid temperature, i.e., 15 K, could hardly produce either detectable protons or neutrons. Even for such cold targets, however, x-ray streak cameras (XSC) and x-ray framing cameras (XFC) caught hot core images as reported [6], yielding hot core

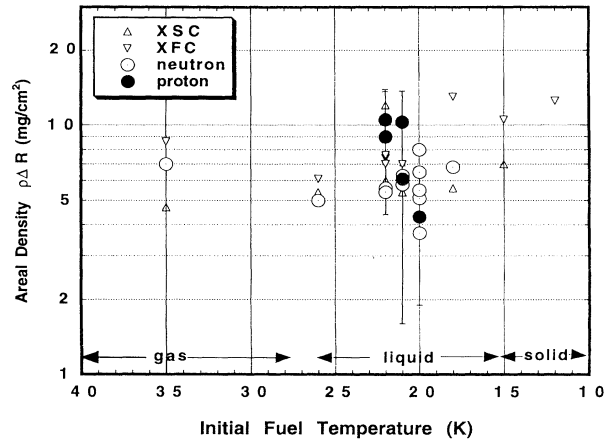


FIG. 3. $\rho \Delta R$ of the second layer (plastic foam and D_2 fuel) from proton energy shift (\bullet) and from the secondary neutron (\circ) versus initial fuel temperature. The error bar on proton is from spectral broadening, and the error bar on neutron is from data scattering between four scintillators. Δ is the core areal density from XSC and ∇ from XFC.

areal densities, assuming uniform fuel compression, as plotted in Fig. 3. The x-ray data suggest that cooling targets down to solid temperature will increase areal densities to about 20 mg/cm^2 .

The maximum x-ray emission takes place at the end of the maximum compression phase at the contact surface between the first and second layers just before it expands [6]. The minimum hot core radius is typically 24 μm , close to the calculated contact surface radius; $R - \Delta R/2 = 18$ μm . The experimental convergence ratio was 12.4 at the contact surface. On increasing the energy E_L from 4 to 12 kJ, both DD and DT yields increase as E_L^4 , keeping the ratio or $\rho \Delta R$ almost constant.

At the maximum compression, the second layer seems to remain and surround the hot core; then the compression is given by $\rho/\rho_0 = (R/\Delta R)(\rho \Delta R)^{3/2}/(R_0^2 \Delta R_0 \rho_0^3)^{1/2}$, where $\rho_0 = 356$ mg/cm^3 . From the x-ray core emission, the imploded shell radius $R \approx 30$ μm [6]. If ΔR is close to the initial shell thickness $\Delta R_0 = 10$ μm , as suggested by the simulation, then $R/\Delta R \approx 3$. Finally, $\rho \Delta R$ of 10.3 ± 3.4 mg/cm^2 for shot No. 12874 gives $\rho = 6.1 \pm 0.9$ g/cm^3 or $\rho/\rho_0 = 17 \pm 2.5$. Typical results are listed in Table I. If the shell structure does not remain, but the fuel is compressed uniformly, then $R/\Delta R \approx 1$, or the density must be roughly one-third of those listed in Table I. The fuel density of GMB (12758) is provided to be $\rho = 50 \pm 20$ mg/cm^3 , or the compression $\rho/\rho_0 = 27$, assuming uniform fuel compression.

The proton $\rho \Delta R$ for 12796-12874 is 1.6 - 1.9 times the neutron $\rho \Delta R$. This gap is explained as follows. The second layer includes not only D_2 but also plastics. Though the secondary neutron method gives only the D_2 $\rho \Delta R$, the proton method gives the total $\rho \Delta R$ of the layer, because any charge can reduce proton energies.

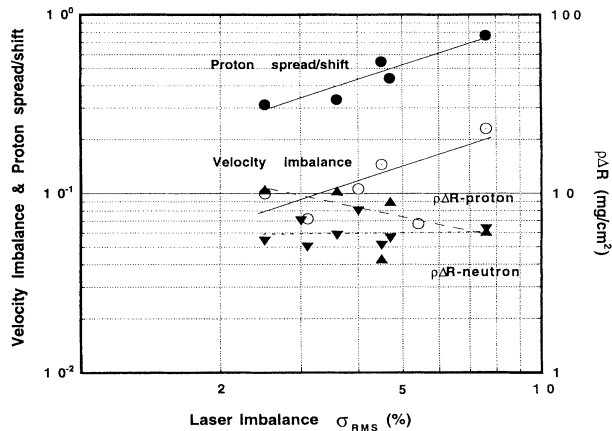


FIG. 4. Implosion velocity imbalance (\diamond), proton energy spread divided by ΔE (\bullet), $\rho\Delta R$ from proton energy shift (\blacktriangle), and $\rho\Delta R$ from secondary neutron (\blacktriangledown) versus laser energy imbalance σ_{rms} (%). Lines are optimal fitted.

The mass ratio of the total layer to the D_2 fraction is $(356 \text{ mg}) / [(0.8 \times 170) \text{ mg}] \cong 2.6$, consistent with the experimental result that the proton $\rho\Delta R$ is 1–2 times the neutron $\rho\Delta R$.

The spectral spreads of the cryogenic target protons are as large as $0.8 \pm 0.2 \text{ MeV}$ (HW of Gaussian curve) or 40%–80% of ΔE as shown in Figs. 1(a) and 1(b). If the protons take not only radial but also tangential paths in the layer, a simple path integration over the shell gives 1.3 times the effective path length, resulting in about 30% geometrical spread, which is less than the experiment. The spread seems to be due to other effects such as laser energy imbalance σ , which can distort the imploding shell symmetry. The velocity imbalance of the imploding shell may bring about an initial shell perturbation at the stagnation. From the in-flight asymmetry of the 1D x-ray image of the imploding shell, we estimated the velocity imbalance of the shell. Figure 4 shows that the velocity imbalance increases with increasing σ_{rms} . The spread divided by ΔE also increases linearly with σ , while, as shown, $\rho\Delta R$ is almost constant or even slowly decreases. $\rho\Delta R$ seems not as sensitive to such a low mode imbalance. It is predicted that the Rayleigh-Taylor

instability at stagnation (deceleration phase) can bring about low mode shell distortion of a few times an initial perturbations [15,16]. If so, the shell distortion grows, possibly resulting in the ΔE spread of the same order of magnitude, since ΔE is proportional to ΔR . In the future, power-balanced laser illumination from the new GEKKO will make the cause of the spectral spreads clearer.

In conclusion, DD protons are used to measure the imploded fuel-shell areal density $\rho\Delta R$, as $\rho\Delta R = 10 \pm 3 \text{ mg/cm}^2$, giving $\rho = 6.1 \pm 0.9 \text{ g/cm}^3$, or the compression $\rho/\rho_0 = 17 \pm 2.5$. The results agree with those from the secondary neutron method within a factor of 2. The proton energy spread is sensitive to the laser energy imbalance.

We acknowledge the GOD and OT groups at the Institute of Laser Engineering for laser operation, the T group for the cryogenic target fabrication, and the MT group for plasma diagnostics. Also we thank R. Ishizaki for stopping-power calculation.

*Permanent address: Commissariat À L'Énergie Atomique, Centre d'Études de Limeil-Valenton, 94195 Villeneuve Saint Georges Cedex, France

- [1] F. J. Marshall *et al.*, Phys. Rev. A **40**, 2547 (1989).
- [2] H. Azechi *et al.*, Laser Part. Beams **9**, 193 (1991).
- [3] Y. Kitagawa *et al.*, Fusion Technol. **21**, 1460 (1992).
- [4] H. Azechi *et al.*, Appl. Phys. Lett. **49**, 55 (1986).
- [5] M. Takagi *et al.*, J. Vac. Sci. Technol. A **11**, 2837 (1993).
- [6] A. Richard *et al.*, Phys. Rev. E **49**, 1520 (1994).
- [7] M. Nakai and T. Yamanaka, Kaku Yugo Kenkyu Suppl. **68**, 79 (1992) (in Japanese).
- [8] T. Norimatsu *et al.*, Rev. Sci. Instrum. **63**, 3378 (1992).
- [9] T. E. Blue *et al.*, J. Appl. Phys. **54**, 615 (1983).
- [10] A. P. Fews *et al.*, Rutherford Appleton Laboratory Annual Report No. RAL-90-026, 1990 (unpublished).
- [11] S. Kacendar *et al.*, Phys. Rev. Lett. **49**, 463 (1982).
- [12] H. Brysk, Plasma Phys. **15**, 611 (1973).
- [13] Y. Kitagawa *et al.*, Phys. Rev. Lett. **56**, 2804 (1986).
- [14] H. Furukawa and K. Nishihara, Phys. Rev. A **46**, 6596 (1992).
- [15] H. Azechi, in Proceedings of ILE NOSE Review '94, Osaka (unpublished).
- [16] N. Miyanaga *et al.*, Jpn. J. Appl. Phys. **22**, L551 (1983).